Journal Pre-proof

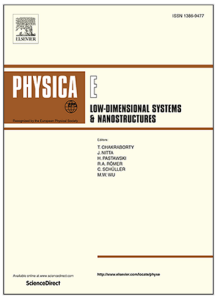

Intra- and inter-band magneto-optical absorption in monolayer WS_2

Pham Thi Huong, Do Muoi, Tran N. Bich, Huynh V. Phuc,
C.A. Duque, Phu Thuong Nhan Nguyen, Chuong V. Nguyen, Nguyen
N. Hieu, Le T. Hoa

PII: S1386-9477(20)30545-2
DOI: https://doi.org/10.1016/j.physe.2020.114315
Reference: PHYSE 114315

To appear in: *Physica E: Low-dimensional Systems and Nanostructures*

Received date : 20 March 2020
Revised date : 10 June 2020
Accepted date : 18 June 2020

Please cite this article as: P.T. Huong, D. Muoi, T.N. Bich et al., Intra- and inter-band magneto-optical absorption in monolayer WS_2, *Physica E: Low-dimensional Systems and Nanostructures* (2020), doi: https://doi.org/10.1016/j.physe.2020.114315.

This is a PDF file of an article that has undergone enhancements after acceptance, such as the addition of a cover page and metadata, and formatting for readability, but it is not yet the definitive version of record. This version will undergo additional copyediting, typesetting and review before it is published in its final form, but we are providing this version to give early visibility of the article. Please note that, during the production process, errors may be discovered which could affect the content, and all legal disclaimers that apply to the journal pertain.

© 2020 Published by Elsevier B.V.

Journal Pre-proof

Intra- and inter-band magneto-optical absorption in monolayer WS_2

Pham Thi Huong [a,b], Do Muoi [c], Tran N. Bich [d,e], Huynh V. Phuc [f], C. A. Duque [g], Phu Thuong Nhan Nguyen [h], Chuong V. Nguyen [i], Nguyen N. Hieu [j,k], Le T. Hoa [j,k,*]

[a] *Division of Computational Mathematics and Engineering, Institute for Computational Science, Ton Duc Thang University, Ho Chi Minh City 758307, Vietnam*

[b] *Faculty of Environment & Labour Safety, Ton Duc Thang University, Ho Chi Minh City 758307, Vietnam*

[c] *University of Science-VNU.HCM, 227-Nguyen Van Cu Street, District 5, Ho Chi Minh City 700000, Viet Nam*

[d] *Division of Physics, Quang Binh University, Quang Binh 510000, Viet Nam*

[e] *Physics Department, University of Education, Hue University, Hue 530000, Viet Nam*

[f] *Division of Theoretical Physics, Dong Thap University, Cao Lanh 870000, Viet Nam*

[g] *Grupo de Materia Condensada-UdeA, Instituto de Física, Facultad de Ciencias Exactas y Naturales, Universidad de Antioquia UdeA, Calle 70 No. 52-21, Medellín, Colombia*

[h] *Center of Excellence for Green Energy and Environmental Nanomaterials, Nguyen Tat Thanh University, Ho Chi Minh City, Viet Nam*

[i] *Department of Materials Science and Engineering, Le Quy Don Technical University, Ha Noi 100000, Viet Nam*

[j] *Institute of Research and Development, Duy Tan University, Da Nang 550000, Viet Nam*

[k] *Faculty of Natural Sciences, Duy Tan University, Da Nang 550000, Viet Nam*

Preprint submitted to Elsevier *9 June 2020*

Journal Pre-proof

Journal Pre-proof

Abstract

In this paper, the optical absorption coefficients (OACs) and the refractive index changes (RICs) due to both intra- and inter-band transitions in monolayer WS_2 are theoretically investigated in the presence of a magnetic field. The results showed that both OACs and RICs display the blue-shift behavior with the increase of the magnetic field. The Zeeman fields have no effect on the peak positions but reduce slightly peak intensities. Besides, the strong spin-orbit coupling in monolayer WS_2 causes the significant difference of the peak due to spin up and down. The OACs and RICs due to intra-band transition display only one peak in the THz range, while the inter-band spectra show a series of peaks in the near-infrared to the visible optical range, making monolayer WS_2 to be a promising candidate for novel optoelectronic applications.

© 2020 Elsevier B.V. All rights reserved.

Key words: Monolayer WS_2, Nonlinear magneto-optical properties, Magnetic field.

1 Introduction

In the last few years, the layered two-dimensional (2D) materials such as graphene [1,2], phosphorene [3], silicene [4,5], germanene [6], and transition-metal dichalcogenides (TMDC) [7–10] have attracted great interest caused by their outstanding properties. These materials have been attracted not only by their fundamental physical properties but also by their great potential applications [11–14]. One of the problems preventing graphene from being a perfect candidate for graphene-based transistors comes from its low on/off ratio, which is caused by the gapless band structure of this interesting material [15]. With their natural large

* Corresponding authors.
Email addresses: phamthihuong@tdtu.edu.vn (Pham Thi Huong),
lethihoa8@duytan.edu.vn (Le T. Hoa).

bandgaps, the TMDCs resolves wonderfully the gapless problem of graphene, gradually emerged as a potential candidate for new generation materials. That is the reason why the TMCDs have attracted wide attention from scientists in recent years. Among them, monolayer tungsten disulfide (WS_2) has been being attracted increasing attention due to its great properties. Firstly, the material WS_2 has strong spin-orbit-coupling (SOC): its values are $\lambda_v = 0.430$ eV and $\lambda_c = 0.029$ eV in the valence band and the conduction band, respectively [16], providing a great system for spin control [17]. Secondly, the band structures of WS_2 displays a pair of incommensurate valleys at the K and K' points. The different conduction and valence bands are spaced by a direct band-gap in the near-infrared to the visible spectral range, which results in the efficiency in the electromagnetic wave absorption and emission.

Another interesting feature of the material WS_2 is its layer dependent characteristics [14]. While the bulk and the multilayer display the indirect-gap semiconductors, the monolayer WS_2 is a direct-gap one with a large energy gap [18]. With the energy gap of $\Delta = 0.90$ eV [19] and the low defect density, the monolayer WS_2 shows strong photoluminescence [20,21]. Therefore, the physical properties of the monolayer WS_2 have been being one of the most subjects studied in recent years, especially when a uniform magnetic field is taken into account [22–24]. The photoluminescence of monolayer WS_2 in the strong magnetic field (up to 30 T) has been measured [22]. The results showed that with increasing magnetic field, the relative rotation angle between the polarization of the exciting light and the photoluminescence emission strongly increases, up to 35° at $B = 25$ T, and lessens the polarization degree of emission. The monolayer WS_2 samples have been studied using photoluminescence spectroscopy [23,24], in which the photoluminescence emission is governed by two types of excitons: (neutral and charged excitons). For the charged excitons, two separate types of them, including singlets and triplets,

have been observed nearby the neutral exciton emission line. These prominent results open a new way to study and exploit the valley-dependent phenomenon, which is really hopeful for novel optoelectronics applications.

In this work, we study optical absorption coefficients (OACs) and the refractive index changes (RICs) generated by the intra- and inter-band transitions in monolayer WS_2 in the presence of a magnetic field. The results are reported for both cases of spin orientation: up and down. We find that both OACs and RICs show blue-shift behavior with a growing magnetic field. Besides, while the optical spectrum due to intraband transition display only one peak in the THz range, the interband spectrum display a series of peaks in the near-infrared to the visible optical range.

2 Theoy

2.1 Single-particle Hamiltonian

We consider a monolayer WS_2 oriented in the (x, y) plane. Including the spin, M_s, and valley, M_v, Zeeman fields into the single-particle Hamiltonian of Ref. [25], we have

$$\hat{H}_0 = v_F(v\sigma_x\pi_x + \sigma_y\pi_y) + \Delta_{v,s}\sigma_z + O_{v,s} + sM_s - vM_v, \tag{1}$$

where $v_F = 6.65 \times 10^5$ m/s is the Fermi velocity [19], $v = \pm 1$ is for the K and K' valleys, $s = \pm 1$ is for spin up and down, $\pi = \mathbf{p} + e\mathbf{A}$ with $\mathbf{p}$ and $\mathbf{A}$ being the momentum and the vector potential of the magnetic field, respectively, $\sigma_{x(y,z)}$ are the Pauli matrices whose eigenvalues are ± 1. The spin and valley Zeeman fields have the same form as $M_{s(v)} = g_{s(v)}\mu_B B/2$ with the Bohr magneton $\mu_B = e\hbar/2m_e$, $g_{s(v)} = 2 + g'_{s(v)}$. Here $g'_s = 0.84$ and $g'_v = 4.96$ are the Landé factors, and $m_e = 0.35m_0$ [26,27]. The expressions for the Dirac mass and the offset

energy are [28]

$$\Delta_{v,s} = \Delta + vs(\lambda_c - \lambda_v)/4, \quad O_{v,s} = vs(\lambda_c + \lambda_v)/4, \tag{2}$$

where $\Delta = 0.90$ eV is the intrinsic band-gap of the material [19]. The eigenfunctions are $|\lambda\rangle = \chi_s \otimes \psi^{v,p}_{n,s}(x)e^{ik_y y}/\sqrt{L_y}$ where χ_s is the eigenfunction of of $\hat{s}_z$ [29], and

$$\psi^{v,p}_{n,s}(x) = \begin{pmatrix} va^{v,p}_{n,s}\phi_{n-1}(x - x_0) \\ \\ b^{v,p}_{n,s}\phi_n(x - x_0) \end{pmatrix}. \tag{3}$$

Here ϕ_n are the usual oscillator functions with the coordinator center $x_0 = \alpha_c^2 k_y$. The index p labels the conduction and valence bands and $n = 0, 1, 2, \ldots$ is the Landau level (LL) index. The normalization coefficients $a^{v,p}_{n,s}$ and $b^{v,p}_{n,s}$ are given by

$$a^{v,p}_{n,s} = \sqrt{\frac{pE^v_{n,s} + \Delta_{v,s}}{2pE^v_{n,s}}}, \; b^{v,p}_{n,s} = \sqrt{\frac{pE^v_{n,s} - \Delta_{v,s}}{2pE^v_{n,s}}}. \tag{4}$$

The corresponding eigenvalues of Eq. (1) are

$$E_\lambda = E^{v,p}_{n,s} = pE^v_{n,s} + O_{v,s} + sM_s - vM_v, \tag{5}$$

where λ is shorthand for $\{\eta, k_y\}$ with $\eta = \{n, s, v, p\}$, $E^v_{n,s} = [n(\hbar\omega)^2 + (\Delta_{v,s})^2]^{1/2}$ with $\omega_c = v_F\sqrt{2}/\alpha_c$ being the cyclotron frequency, $\alpha_c = (\hbar/eB)^{1/2}$. Using the relation $\hbar\omega_c \ll \Delta_{v,s}$, we have $E^v_{n,s} \approx \Delta_{v,s} + n(\hbar\omega_c)^2/(2\Delta_{v,s})$, therefore, the eigenvalues in Eq. (5) can be written as follows

$$E_\lambda \approx np\frac{(\hbar\omega_c)^2}{2\Delta_{v,s}} + p\Delta_{v,s} + O_{v,s} + sM_s - vM_v. \tag{6}$$

Since $(\hbar\omega_c)^2 \sim B$, Eq. (6) shows a linear increase of the LLs spectrum on the field and the LL index in both conduction and valence bands. For $n = 0$, we have $\psi^K_{0,s} = (0, \phi_0)^{Tr}$ and $\psi^{K'}_{0,s} = (\phi_0, 0)^{Tr}$ with Tr being the transpose. The corresponding

eigenvalues for $n = 0$ are

$$E_{0,s}^{K} = -\Delta + s\lambda_v/2 + sM_s - M_v, \tag{7}$$

$$E_{0,s}^{K'} = \Delta - s\lambda_c/2 + sM_s + M_v. \tag{8}$$

Note that, the eigenfunctions and eigenvalues obtained here could be also obtained from Ref. [30] in the case of absence electric field.

2.2 *Dipole matrix element*

When the system is considered to excite by an incident light $E(t) = \tilde{E}e^{i\Omega t} + \tilde{E}e^{-i\Omega t}$, the total Hamiltonian can be written as

$$\hat{H} = \hat{H}_0 + \hat{H}_{int}, \tag{9}$$

where $\hat{H}_0$, which is shown in Eq. (1), is the unperturbed Hamiltonian part and

$$\hat{H}_{int} = -\hat{d} \cdot E(t) \tag{10}$$

is the perturbed Hamiltonian part, which describes the dipole interaction between system with the light. Here, $\hat{d} = -e\hat{r}$ is the dipole matrix operator with $\hat{r} = (\hat{x}, \hat{y})$ the 2D position operator. For the dipole matrix element in the x-direction, we have

$$\begin{aligned} d_{\lambda',\lambda}^{x} &= -e\delta_{k_y,k_y'}\langle\psi_{n',s'}^{v',p'}|x|\psi_{n,s}^{v,p}\rangle \\ &= -e\delta_{k_y,k_y'}\frac{\langle\psi_{n',s'}^{v',p'}|[H_0,x]|\psi_{n,s}^{v,p}\rangle}{E_{\lambda'} - E_{\lambda}}. \end{aligned} \tag{11}$$

where the commutator is $[H_0, x] = -i\hbar v_F v\sigma_x$. Therefore, the dipole matrix element is derived

$$d_{\lambda',\lambda}^{x} = \frac{ie\hbar v_F v}{E_{\lambda',\lambda}}\left[(v')^*(a_{n',s'}^{v',p'})^* b_{n,s}^{v,p}\delta_{n',n+1} + v(b_{n',s'}^{v',p'})^* a_{n,s}^{v,p}\delta_{n',n-1}\right]\delta_{k_y'k_y}, \tag{12}$$

where $E_{\lambda',\lambda} = E_{\lambda'} - E_{\lambda}$ is the energy different between the two electronic sates $|\lambda'\rangle$ and $|\lambda\rangle$. Eq. (12) implies that the selection rule for the allowed transitions is

Journal Pre-proof

$\Delta n = \pm 1$ and at the same k_y points, agreeing with that in graphene [31–36], in silicene [37–39], and in the transition metal dichalcogenides monolayer [30,40].

2.3 The absorption coefficients and the refractive index changes

When the matrix density is solved in a series in powers of the incident light, the optical polarization in the x-direction of the system, $P_{xx}(t) = (1/V)\mathrm{Tr}(\hat{\rho} \cdot \hat{d})$, can be usually expanded in terms of electric susceptibilities [31,32,41]. The time-evolution equation for the density matrix elements if given by

$$\frac{\partial \rho_{\lambda',\lambda}}{\partial t} = -\frac{i}{\hbar}[\hat{H}_0 + \hat{H}_{int}, \hat{\rho}]_{\lambda',\lambda} - \gamma_{\lambda',\lambda}(\rho_{\lambda',\lambda} - \rho^{(eq)}_{\lambda',\lambda}). \tag{13}$$

Here the term $\gamma_{\lambda',\lambda}$ is a phenomenological decay rate, which describes the relaxation of $\rho_{\lambda',\lambda}$ to its equilibrium value $\rho^{(eq)}_{\lambda',\lambda}$. Eq. (13) is solved using an iterative approach [42–47], $\rho_{\lambda',\lambda}(t) = \sum_n \rho^{(n)}_{\lambda',\lambda}(t)$, with

$$\frac{\partial \rho^{(n)}_{\lambda',\lambda}}{\partial t} = -(i\omega_{\lambda',\lambda} + \gamma_{\lambda',\lambda})\rho^{(n)}_{\lambda',\lambda} - \frac{i}{\hbar}[\hat{H}_{int}, \hat{\rho}^{(n-1)}]_{\lambda',\lambda}, \tag{14}$$

where we have denoted $\omega_{\lambda',\lambda} = E_{\lambda',\lambda}/\hbar$.

On the other hand, the electronic polarization can be expanded into series as follows [44–47]

$$P(t)_{ij} \approx \epsilon_0 \chi^{(1)}_{ij}(\Omega)\tilde{E}e^{i\Omega t} + \epsilon_0 \chi^{(3)}_{ij}(\Omega)\tilde{E}^2\tilde{E}e^{i\Omega t}, \tag{15}$$

where ϵ_0 is the permittivity of vacuum and Ω is the frequency of the incident electromagnetic field. In Eq. (15), $\chi^{(1)}_{ij}(\Omega)$ and $\chi^{(3)}_{ij}(\Omega)$ are, respectively, the linear and third-nonlinear susceptibilities. Using the procedure suggested by Ahn and Chuang [42,43], the linear longitudinal susceptibility in the 2D systems is given by [31,32,41]

$$\epsilon_0 \chi^{(1)}_{xx}(\Omega) = \frac{1}{V}\sum_{\eta',\eta}\sum_{k'_y,k_y} \frac{(f_\lambda - f_{\lambda'})(d^x_{\lambda',\lambda})^* d^x_{\lambda',\lambda}}{E_{\lambda'\lambda} - \hbar\Omega - i\hbar\gamma}, \tag{16}$$

where $f_\lambda = \rho^{(0)}_{\lambda,\lambda}$ is the Fermi-Dirac distribution function for the $|\lambda\rangle$ state. Using the relation $\sum_{k_y} \to (L_y/2\pi)\int_{-L_x/2\alpha_c^2}^{L_x/2\alpha_c^2} = S_0/2\pi\alpha_c^2$, the expression for the 2D linear longitudinal optical susceptibility is found

$$\epsilon_0\chi^{(1)}_{xx}(\Omega) = \frac{1}{2\pi h\alpha_c^2}\sum_{\eta',\eta}\frac{(f_\lambda - f_{\lambda'})(d^x_{\lambda',\lambda})^* d^x_{\lambda',\lambda}}{E_{\lambda'\lambda} - \hbar\Omega - i\hbar\gamma}, \tag{17}$$

where $h = V/S_0 = 3.14$ Å [48] is the thickness of the monolayer WS_2. Following analogous procedure, the expression for the third-order nonlinear longitudinal susceptibility can be obtained as follows

$$\epsilon_0\chi^{(3)}_{xx}(\Omega) = -\frac{1}{2\pi h\alpha_c^2}\sum_{\eta',\eta}\frac{(d^x_{\lambda',\lambda})^* d^x_{\lambda',\lambda}(f_\lambda - f_{\lambda'})}{E_{\lambda',\lambda} - \hbar\Omega - i\hbar\gamma_0}\left[\frac{4(d^x_{\lambda',\lambda})^* d^x_{\lambda',\lambda}}{(E_{\lambda',\lambda} - \hbar\Omega)^2 + (\hbar\gamma_0)^2}\right.$$
$$\left. - \frac{(d^x_{\lambda',\lambda'} - d^x_{\lambda,\lambda})^2}{(E_{\lambda',\lambda} - i\hbar\gamma_0)(E_{\lambda',\lambda} - \hbar\Omega - i\hbar\gamma_0)}\right]. \tag{18}$$

The longitudinal susceptibilities $\chi^{(n)}_{xx}(\Omega)$ are related to the OACs and RICs by [44–46]

$$\alpha^{(n)}(\Omega) = \Omega\sqrt{\frac{\mu}{\varepsilon_R}}\mathrm{Im}\left[\epsilon_0\chi^{(n)}_{xx}(\Omega)\tilde{E}^{(n-1)}\right], \tag{19}$$

$$\frac{\Delta n^{(n)}(\Omega)}{n_r} = \mathrm{Re}\left[\frac{\chi^{(n)}_{xx}(\Omega)\tilde{E}^{(n-1)}}{2n_r^2}\right], \tag{20}$$

where $n = 1, 3$ referring to the linear and nonlinear terms, respectively, μ is the material permeability, and $\varepsilon_R = n_r^2\epsilon_0$ with $n_r = 6.25$ being the material refractive index [49]. Therefrom, the total OAC and the total RIC can be written as [44–46]

$$\alpha(\Omega, I) = \alpha^{(1)}(\Omega) + \alpha^{(3)}(\Omega, I) \tag{21}$$

$$\frac{\Delta n(\Omega, I)}{n_r} = \frac{\Delta n^{(1)}(\Omega)}{n_r} + \frac{\Delta n^{(3)}(\Omega, I)}{n_r}, \tag{22}$$

where $I = 2\epsilon_0 n_r c|\widetilde{E}|^2$ is the light intensity with c being the velocity of light in the vacuum.

3 Results and discussion

We now evaluate numerically the linear and nonlinear OACs and RICs in monolayer WS_2. The parameters of materials are shown when they appeared, the others are as follows: $I = 5 \times 10^6$ W/m^2 and $\hbar\Gamma = 0.2\sqrt{B}$ meV [36]. The 2D density of 2×10^{12} cm^{-2} [50] results in the Fermi energy of 109.8 meV. Because the K and K' valleys are symmetric each other through their reversed spin indices, i.e., $K\uparrow(\downarrow) = K'\downarrow(\uparrow)$ [30], we only evaluate for the K and put $v = v' = 1$.

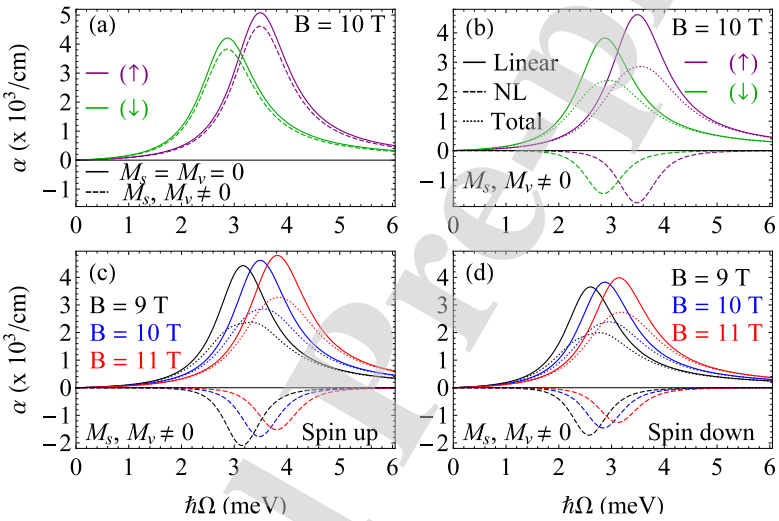

Fig. 1. The OACs for intraband transitions versus photon energy including the effects of spin, valley Zeeman and magnetic fields: (a) with and without Zeeman fields, (b) the linear, nonlinear and total OACs, (c) OACs due to spin-up case for different magnetic fields, and (d) the same as those in (c) but for spin down.

In Fig. 1, the OACs caused by intraband transitions $(p = p' = 1)$ are presented as a function of $\hbar\Omega$ for different effects. The allowed transitions obey the condition $\Delta n = n' - n = \pm 1$, which leads to the energy difference $E_{\lambda',\lambda} = (\hbar\omega_c)^2/(2\Delta_{1,s})$. It is clear that $E_{\lambda',\lambda}$ is independent of the LL index and has the same value for all the intraband transitions at given values of B and s. Therefore, the OACs peak

caused by intraband transition, which satisfy the condition

$$\hbar\Omega_{intra} = \frac{(\hbar\omega_c)^2}{2\Delta_{1,s}} = \frac{(\hbar\omega_c)^2}{2[\Delta + s(\lambda_c - \lambda_v)/4]}, \tag{23}$$

locate at the same position, generating only one peak, for one value of the magnetic field and spin index as shown in all panels of Fig. 1. This result disagrees with that in graphene where the LL spectrum is found to be proportional to $\sqrt{n}$ [36], but agrees with that reported in monolayer MoS_2 [40] and in phosphorene [51]. This is because, in all monolayers of WS_2, MoS_2, and phosphorene, the LL spectrum is linearly proportional to n. It can be seen from Fig. 1(a) that when the Zeeman fields are taken into account, the peak positions do not change but their intensities slightly reduce. Besides, the strong SOC in monolayer WS_2 results in the significant difference of the peak positions due to spin-up and spin-down. From the relation $\lambda_c - \lambda_v = -0.401$ eV< 0, we have $\Delta_{1,+1} < \Delta_{1,-1}$. Using this into Eq. (23) we find that $\hbar\Omega_{intra}(s = +1) > \hbar\Omega_{intra}(s = -1)$, this explains the fact that in the intraband transitions, the peaks due to spin-up are always at the right-hand side of those due to spin-down. In Fig. 1(b) we show the dependence of the linear, the third-order nonlinear, and the total OACs for intraband transition on the $\hbar\Omega$ at $B = 10$ T, including the effect of Zeeman fields. Because of its negative value, the contribution of the nonlinear term pull the value of the total term downs, matching the results reported in the literature [52–55]. Figures 1(c) and 1(d) illustrate the dependence of the OACs on photon energy for the different magnetic fields for spins up and down. With the enhancement of the field, the OAC spectra shift to higher energy region because of the increase of cyclotron energy. For the OACs intensities, while the third-order nonlinear reduces, the linear and the total terms increase when the magnetic field increases in both spins up and down. The increase of the total OAC is in agreement with that reported in monolayer phosphorene [51] and MoS_2 [40], and in conventional low-dimensional system [56].

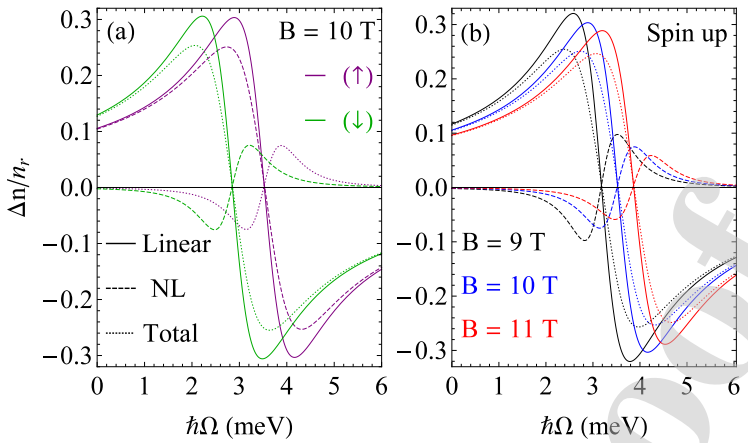

Fig. 2. The RICs for intraband transitions versus photon energy: (a) the linear, nonlinear and total RICs for spin up and down, (b) RICs due to spin-up case for different magnetic fields. The results are calculated for $M_s, M_v \neq 0$.

In Fig. 2(a), the linear, third-order nonlinear, and total RICs are displayed as functions of photon energy at $B = 10$ T. Similar to the case of OACs, the absorbed photon energies due to intraband transitions here are also in the THz range, just like the optical Hall conductivity in graphene [57], in silicene [37] and like the magneto-optical conductivity in Weyl semimetals [58], and in topological insulator [59]. Besides, the relation between the absorbed photon energies caused by spin-up and the spin-down cases as well as the reduction of the nonlinear part to the total are also observed in monolayer WS_2, similarly to those in MoS_2 [40]. One can see from Fig. 1(b) and Fig. 2(a) that the behavior of OACs and RICs caused by the spin-up and the spin-down cases are the same. In the following, we only evaluate the spin-up, but the results are also true for the other case. In Fig. 2(b), we illustrate the dependence of the RICs on $\hbar\Omega$ for different magnetic fields. Similar to the OACs, the increase of the energy different, $E_{\lambda',\lambda}$, with the strong magnetic field causes the blue-shift feature of the RICs. Meanwhile, the drop in the RICs intensities is the cause of the reduction of the dipole matrix element, $d^x_{\lambda'\lambda}$ when the magnetic field increases. This can be explained clearly form Eq. (12): the increase of B leads to

the increase of $E_{\lambda',\lambda}$ and therefore, leads to the drop of the dipole matrix element.

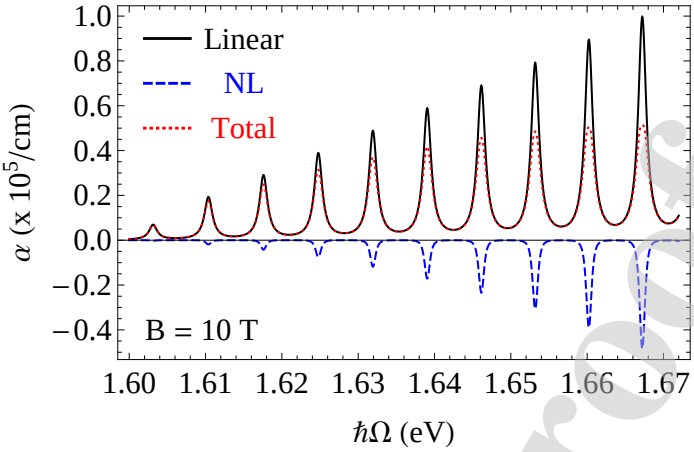

Fig. 3. The OACs for interband transitions versus photon energy at $B = 10$ T. The results are evaluated for spin-up case and $M_s, M_v \neq 0$.

The variation of the OACs due to interband transitions ($p = -1 \rightarrow p = 1$) on the photon energy is presented in Fig. 3. It can be seen that (i) the interband transitions peaks appear in a series and (ii) locate in the near-infrared to visible regime. These features can be explained from the expression of the absorbed photon energies for the interband transitions as follows

$$\begin{aligned}\hbar\Omega_{inter} &= (2n+1)\frac{(\hbar\omega_c)^2}{2\Delta_{1,s}} + 2\Delta_{1,s}, \\ &= \frac{(2n+1)(\hbar\omega_c)^2}{2[\Delta + s(\lambda_c - \lambda_v)/4]} + 2\left[\Delta + s\frac{\lambda_c - \lambda_v}{4}\right]. \end{aligned} \tag{24}$$

Firstly, because $\hbar\Omega_{inter}$ is proportional to $(2n+1)$, the peak positions caused by different LL indexes are not overlapped, they gradually move to the right-hand side with the bigger LL indexes, generating a series of the resonant peaks. Secondly, Eq. (24) reveals that $\hbar\Omega_{inter} \sim 2\Delta_{1,1} = 1.5995$ eV ($s = 1$ for spin up case). Therefore, the peaks due to interband transitions are at the near-infrared to visible regime, agreeing with previous study for monolayer WS_2 [60]. Note that, while the first peak is generated by only one transition from $n = 0$ to $n' = 1$, the others are doubled. For example, the second peak is the result of the interband transi-

tions from $n = 1$ to $n' = 2$ and from $n = 2$ to $n' = 1$, or written in the short form as $1(2) \rightarrow 2(1)$. It is clear that these two transitions have the same photon absorbed energy, therefore, they appear at the same position, displaying only one peak for each couple-interband-transition. The higher-order interband transition peaks, $2(3) \rightarrow 3(2),\ 3(4) \rightarrow 4(3), \ldots$, are also generated by the same way. Besides, the intensities of the interband transitions, here in monolayer WS_2, are much bigger than that of intraband transitions. This is in contrast to the behavior of the optical conductivity in black phosphorus thin films [61], in monolayer silicene [62], in bilayer transition metal dichalcogenides [63], but in agreement with that of OACs in monolayer graphene [36] and in monolayer MoS_2 [40].

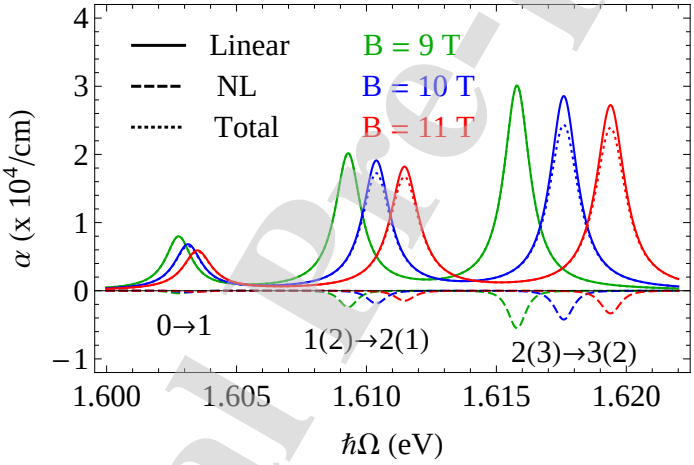

Fig. 4. The OACs for first-three interband transitions versus photon energy for different magnetic fields. The results are calculated for spin-up case and $M_s, M_v \neq 0$.

In Fig. 4, the OACs for the first-three interband transitions are presented as functions of $\hbar\Omega$ for different magnetic fields. Similar to the intraband transition case (see Fig. 1c), we also observe that when the magnetic field increases, the OAC peaks reduce in the intensity and shift to the right-hand side. The physical meaning is explained exactly the same way as done in the intraband transitions, i.e., the intensity reduction and the blue-shift are the result of the enhancement of transition energies, $E_{\lambda',\lambda}$ when magnetic field increases from 9 T to 11 T.

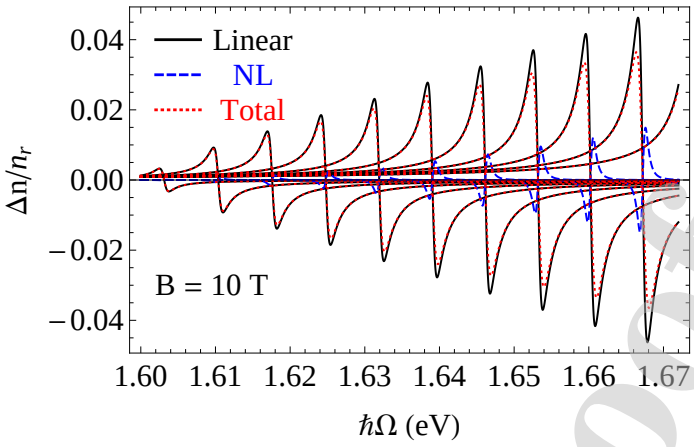

Fig. 5. The RICs for interband transitions versus photon energy at $B = 10$ T. The results are evaluated for spin-up case and $M_s, M_v \neq 0$.

In Fig. 5, we show the RICs for the interband transition in monolayer WS_2 as a function of $\hbar\Omega$ at $B = 10$ T. The results are evaluated for spin-up cases only, including the effect of Zeeman fields. In comparison to the OACs, the RICs due to interband transitions also display a series of peaks but have smaller intensities in comparison to the intraband transitions. Besides, we can see from Eq. (12) that the term $d^x_{\lambda',\lambda}$ increases with the LL index, resulting in the enhancement of the interband RICs as observed in Fig. 5. These results are in agreement with previous works reported in graphene [36] and monolayer MoS_2 [40].

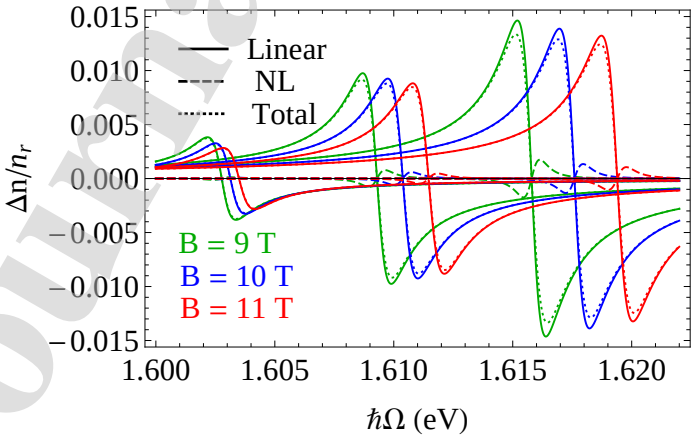

Fig. 6. The RICs for first-three interband transitions versus photon energy for different magnetic fields. The results are evaluated for spin-up case and $M_s, M_v \neq 0$.

In Fig. 6, we show the RICs for first-three interband transitions ($0 \rightarrow 1$, $1(2) \rightarrow 2(1)$, and $2(3) \rightarrow 3(2)$) as functions of $\hbar\Omega$ for different magnetic fields. We can see that when the magnetic field increases the RICs due to interband transitions display a blue-shift and reduce the intensities. The values of interband RICs here are much bigger than those in phosphorene [51] and graphene [36] but in the same order of magnitude as that in monolayer MoS_2 [40]. This is because both MoS_2 and WS_2 are the members of a new two-dimensional material type: transition metal dichalcogenides, which have large nature band-gap and strong spin-orbit interaction, leading to the stronger dipole matrix element in these materials in comparison to that in graphene and phosphorene.

4 Conclusions

We have studied the linear, the third-order nonlinear, and the total OACs and RICs for both intra- and inter-band transitions in monolayer WS_2. The Zeeman fields have no effect on the peak positions but reducing peak intensities. The strong SOC in monolayer WS_2 makes the resonant peaks due to spin-up and spin-down different, where the peaks due to spin-up cases are always at the right-hand side of those due to spin down. The magnetic field gives a significant effect on the OACs and the RICs; both of them make a blue-shift and reduce the total intensities when the magnetic field becomes stronger. The allowed transitions satisfy the condition $\Delta n = n' - n = \pm 1$. For the intraband transitions, the absorbed photon energies are defined by $\hbar\Omega_{intra} = (\hbar\omega_c)^2/(2\Delta_{1,s})$ which display only one resonant peak in the THz region. Meanwhile, since the absorbed photon energies depend on the LL index, $\hbar\Omega_{inter} = (2n+1)(\hbar\omega_c)^2/(2\Delta_{1,s}) + 2\Delta_{1,s}$, the interband transitions show a series of peaks. Besides, because of the large nature bandgap of monolayer WS_2, the interband transitions peaks in this material located in the near-infrared

to the visible regime. This makes monolayer WS_2 to be a promising material for application in optoelectronic devices.

Acknowledgments

This research is funded by Vietnam National Foundation for Science and Technology Development (NAFOSTED) under Grant number 103.01-2019.11, and Quang Binh University under Grant No. CS.10.2020. CAD acknowledges the financial support from *El Patrimonio Autónomo Fondo Nacional de Financiamiento para la Ciencia, la Tecnología y la Innovación Francisco José de Caldas* (project: CD 111580863338, CT FP80740-173-2019).

References

[1] K. S. Novoselov, D. Jiang, F. Schedin, T. J. Booth, V. V. Khotkevich, S. V. Morozov, A. K. Geim, Proc. Natl. Acad. Sci. USA 102 (2005) 10451.

[2] N. M. R. Peres, Rev. Mod. Phys. 82 (2010) 2673.

[3] M. Tahir, P. Vasilopoulos, F. M. Peeters, Phys. Rev. B 92 (2015) 045420.

[4] P. Vogt, P. De Padova, C. Quaresima, J. Avila, E. Frantzeskakis, M. C. Asensio, A. Resta, B. Ealet, G. Le Lay, Phys. Rev. Lett. 108 (2012) 155501.

[5] L. Chen, C.-C. Liu, B. Feng, X. He, P. Cheng, Z. Ding, S. Meng, Y. Yao, K. Wu, Phys. Rev. Lett. 109 (2012) 056804.

[6] X. Chen, Q. Yang, R. Meng, J. Jiang, Q. Liang, C. Tan, X. Sun, J. Mater. Chem. C 4 (2016) 5434.

[7] L. Guo, M. Wu, T. Cao, D. M. Monahan, Y.-H. Lee, S. G. Louie, G. R. Fleming, Nat. Phys. 15 (2019) 228.

Journal Pre-proof

[8] M. M. Glazov, M. A. Semina, C. Robert, B. Urbaszek, T. Amand, X. Marie, Phys. Rev. B 100 (2019) 041301(R).

[9] D. Van Tuan, A. M. Jones, M. Yang, X. Xu, H. Dery, Phys. Rev. Lett. 122 (2019) 217401.

[10] J. Knörzer, M. J. A. Schuetz, G. Giedke, D. S. Wild, K. De Greve, R. Schmidt, M. D. Lukin, J. I. Cirac, Phys. Rev. B 101 (2020) 125101.

[11] K. F. Mak, J. Shan, Nat. Photonics 10 (2016) 216.

[12] F. Liu, J. Zhou, C. Zhu, Z. Liu, Adv. Funct. Mater. 27 (2017) 1602404.

[13] H. Hong, C. Liu, T. Cao, C. Jin, S. Wang, F. Wang, K. Liu, Adv. Mater. Interfaces 4 (2017) 1601054.

[14] C. Cong, J. Shang, Y. Wang, T. Yu, Adv. Opt. Mater. 6 (2018) 1700767.

[15] K. S. Novoselov, A. K. Geim, S. V. Morozov, D. Jiang, Y. Zhang, S. V. Dubonos, I. V. Grigorieva, A. A. Firsov, Science 306 (2004) 666.

[16] G.-B. Liu, W.-Y. Shan, Y. Yao, W. Yao, D. Xiao, Phys. Rev. B 88 (2013) 085433.

[17] S. Ulstrup, A. G. c. v. a. c. Čabo, D. Biswas, J. M. Riley, M. Dendzik, C. E. Sanders, M. Bianchi, C. Cacho, D. Matselyukh, R. T. Chapman, E. Springate, P. D. C. King, J. A. Miwa, P. Hofmann, Phys. Rev. B 95 (2017) 041405(R).

[18] W. Zhao, Z. Ghorannevis, L. Chu, M. Toh, C. Kloc, P.-H. Tan, G. Eda, ACS Nano 7 (2013) 791.

[19] D. Xiao, G.-B. Liu, W. Feng, X. Xu, W. Yao, Phys. Rev. Lett. 108 (2012) 196802.

[20] H. R. Gutiérrez, N. Perea-López, A. L. Elías, A. Berkdemir, B. Wang, R. Lv, F. López-Urías, V. H. Crespi, H. Terrones, M. Terrones, Nano Lett. 13 (2013) 3447.

[21] L. Yuan, L. Huang, Nanoscale 7 (2015) 7402.

[22] R. Schmidt, A. Arora, G. Plechinger, P. Nagler, A. Granados del Águila, M. V. Ballottin, P. C. M. Christianen, S. Michaelis de Vasconcellos, C. Schüller, T. Korn, R. Bratschitsch, Phys. Rev. Lett. 117 (2016) 077402.

[23] G. Plechinger, P. Nagler, A. Arora, R. Schmidt, A. Chernikov, A. G. del Águila, P. C. M. Christianen, R. Bratschitsch, C. Schüller, T. Korn, Nat. Commun. 7 (2016) 12715.

[24] G. Plechinger, P. Nagler, A. Arora, A. Granados del Águila, M. V. Ballottin, T. Frank, P. Steinleitner, M. Gmitra, J. Fabian, P. C. M. Christianen, R. Bratschitsch, C. Schüller, T. Korn, Nano Lett. 16 (2016) 7899.

[25] G. Catarina, J. Have, J. Fernández-Rossier, N. M. R. Peres, Phys. Rev. B 99 (2019) 125405.

[26] M. Tahir, P. Vasilopoulos, F. M. Peeters, Phys. Rev. B 93 (2016) 035406.

[27] A. Kormányos, V. Zólyomi, N. D. Drummond, G. Burkard, Phys. Rev. X 4 (2014) 011034.

[28] H. Ochoa, R. Roldán, Phys. Rev. B 87 (2013) 245421.

[29] C. M. Wang, X. L. Lei, Phys. Rev. B 92 (2015) 125303.

[30] N. D. Hien, C. V. Nguyen, N. N. Hieu, S. S. Kubakaddi, C. A. Duque, M. E. Mora-Ramos, L. Dinh, T. N. Bich, H. V. Phuc, Phys. Rev. B 101 (2020) 045424.

[31] X. Yao, A. Belyanin, Phys. Rev. Lett. 108 (2012) 255503.

[32] X. Yao, A. Belyanin, J. Phys.: Condens. Matter 25 (2013) 054203.

[33] V. Gusynin, S. Sharapov, J. Carbotte, Phys. Rev. Lett. 98 (2007) 157402.

[34] H. V. Phuc, N. N. Hieu, Opt. Commun. 344 (2015) 12.

[35] H. V. Phuc, L. Dinh, Mater. Chem. Phys. 163 (2015) 116.

Journal Pre-proof

[36] C. V. Nguyen, N. N. Hieu, C. A. Duque, N. A. Poklonski, V. V. Ilyasov, N. V. Hieu, L. Dinh, Q. K. Quang, L. V. Tung, H. V. Phuc, Opt. Mater. 69 (2017) 328.

[37] C. J. Tabert, E. J. Nicol, Phys. Rev. Lett. 110 (2013) 197402.

[38] K. Shakouri, P. Vasilopoulos, V. Vargiamidis, F. M. Peeters, Rev. B 90 (2014) 125444.

[39] D. Muoi, N. N. Hieu, C. V. Nguyen, B. D. Hoi, H. V. Nguyen, N. D. Hien, N. A. Poklonski, S. S. Kubakaddi, H. V. Phuc, Phys. Rev. B 101 (2020) 205408.

[40] C. V. Nguyen, N. N. Hieu, D. Muoi, C. A. Duque, E. Feddi, H. V. Nguyen, L. T. T. Phuong, B. D. Hoi, H. V. Phuc, J. Appl. Phys. 123 (2018) 034301.

[41] X. Yao, Ph.D. thesis, Texas A & M University (2014).

[42] D. Ahn, S.-l. Chuang, IEEE J. Quantum Electron. QE-23 (1987) 2196.

[43] D. Ahn, S. L. Chuang, J. Appl. Phys. 62 (1987) 3052.

[44] Y.-B. Yu, S.-N. Zhu, K.-X. Guo, Solid State Commun. 139 (2006) 76.

[45] B. Chen, K.-X. Guo, R.-Z. Wang, Z.-H. Zhang, Z.-L. Liu, Solid State Commun. 149 (2009) 310.

[46] G. Rezaei, M. J. Karimi, A. Keshavarz, Physica E 43 (2010) 475.

[47] C. M. D. Jiménez, Ph.D. thesis, Universidad de Antioquia (2015).

[48] Y. Ding, Y. Wang, J. Ni, L. Shi, S. Shi, W. Tang, Physica B 406 (2011) 2254.

[49] H.-L. Liu, C.-C. Shen, S.-H. Su, C.-L. Hsu, M.-Y. Li, L.-J. Li, Appl. Phys. Lett. 105 (2014) 201905.

[50] E. J. Sie, A. Steinhoff, C. Gies, C. H. Lui, Q. Ma, M. Rösner, G. Schönhoff, F. Jahnke, T. O. Wehling, Y.-H. Lee, J. Kong, P. Jarillo-Herrero, N. Gedik, Nano Lett. 17 (2017) 4210.

[51] C. V. Nguyen, N. N. Hieu, C. A. Duque, D. Q. Khoa, N. V. Hieu, L. V. Tung, H. V. Phuc, J. Appl. Phys. 121 (2017) 045107.

Journal Pre-proof

[52] E. Al, F. Ungan, U. Yesilgul, E. Kasapoglu, H. Sari, I. Sökmen, Opt. Mater. 47 (2015) 1.

[53] C. M. Duque, A. L. Morales, M. E. Mora-Ramos, C. A. Duque, J. Lumin. 143 (2013) 81.

[54] E. Ozturk, I. Sokmen, J. Lumin. 145 (2014) 387.

[55] N. Aghoutane, M. El-Yadri, A. El Aouami, E. Feddi, F. Dujardin, M. El Haouari, C. A. Duque, C. V. Nguyen, H. V. Phuc, Appl. Phys. A 125 (2018) 17.

[56] M. Gambhir, M. Kumar, P. Jha, M. Mohan, J. Lumin. 143 (2013) 361.

[57] T. Morimoto, Y. Hatsugai, H. Aoki, Phys. Rev. Lett. 103 (2009) 116803.

[58] P. E. C. Ashby, J. P. Carbotte, Phys. Rev. B 87 (2013) 245131.

[59] Z. Li, J. P. Carbotte, Phys. Rev. B 88 (2013) 045414.

[60] A. M. Rivera, A. P. S. Gaur, S. Sahoo, R. S. Katiyar, J. Appl. Phys. 120 (2016) 105102.

[61] X. Zhou, W.-K. Lou, F. Zhai, K. Chang, Phys. Rev. B 92 (2015) 165405.

[62] C. J. Tabert, E. J. Nicol, Phys. Rev. B 88 (2013) 085434.

[63] M. Zubair, M. Tahir, P. Vasilopoulos, Phys. Rev. B 98 (2018) 155402.

Journal Pre-proof

Journal Pre-proof

Highlights

- Optical spectra display the blue-shift behavior when the magnetic field increase.
- The Zeeman fields do not affect the peak positions but reduce slightly their intensities.
- The strong SOC in monolayer WS_2 causes the significant difference of the peak due to spin up and down.
- Peaks due to intraband transitions are in the THz range.
- The interband spectra show a series of peaks in the near-infrared to the visible optical range.

Journal Pre-proof

Journal Pre-proof

AUTHORSHIP STATEMENT

Manuscript Title: Intra- and inter-band magneto-optical absorption in monolayer WS_2

Journal: Physica E: Low-dimensional Systems and Nanostructures

Authors: Pham Thi Huong, Do Muoi, Tran N. Bich, Huynh V. Phuc, C. A. Duque, Phu Thuong Nhan Nguyen, Chuong V. Nguyen, Nguyen N. Hieu and Le T. Hoa

Authors' contributions

Pham Thi Huong: Investigation, Validation, Writing – review & editing**. Do Muoi**: Investigation, Validation. **Tran N. Bich**: Investigation, Validation. **Huynh V. Phuc**: Investigation, Writing - original draft, Writing - review & editing. **C. A. Duque**: Investigation, Validation. **Phu Thuong Nhan Nguyen**: Investigation, Validation. **Chuong V. Nguyen**: Conceptualization, Investigation, Validation. **Nguyen N. Hieu**: Investigation, Validation, Funding acquisition, Writing – original draft. **Le T. Hoa**: Investigation, Writing - original draft, Writing – review & editing.

All authors commented on the manuscript and approved the final manuscript.

On behalf of co-authors

Corresponding author

Huynh V. Phuc
Dong Thap University
Viet Nam

Journal Pre-proof

Declaration of interests

☒ The authors declare that they have no known competing financial interests or personal relationships that could have appeared to influence the work reported in this paper.

☐The authors declare the following financial interests/personal relationships which may be considered as potential competing interests:

Journal Pre-proof